



# Numerical Study on the Effect of Single Shallow Circumferential Groove Casing Treatment on the Flow Field and the Stability of a Transonic Compressor

M. Agha Seyed Mirzabozorg, M. Bazazzadeh and M. Hamzadeh<sup>†</sup>

Department of Aerospace Engineering, Malek Ashtar University of Technology, Isfahan, Iran

<sup>†</sup>Corresponding Author Email: [hamzadeh@mut-es.ac.ir](mailto:hamzadeh@mut-es.ac.ir)

(Received April 30, 2016; accepted September 23, 2016)

## ABSTRACT

The present research investigates the effect of the location and the width of single shallow circumferential groove casing treatment on the flow field and the stability improvement of NASA Rotor 37 utilizing the help of computational fluid dynamics. At first, steady state simulation of Rotor37 was presented for smooth casing (without groove). Then, forty five various grooved casing were simulated and compared with the smooth casing. The results indicated that narrow grooves had slight effect on the adiabatic efficiency but as the width of the groove was increased, a decline in efficiency was observed. The investigation on the stall margin revealed that narrow grooves next to the leading edge could improve the stall margin by a reduction in the size of vortex breakdown zone. Medium-width grooves displayed an effective role in delaying the separation- produced by shock wave and boundary layer interaction- on the blade suction side near the casing. This type of grooves could improve the stall margin more than narrow grooves when located on the top of separation zone near the blade suction side. Wide grooves had negative effect on the stall margin and caused a significant drop in the efficiency and the total pressure ratio of the compressor.

**Keywords:** Circumferential groove; Transonic compressor; Stall margin; CFD.

## NOMENCLATURE

a	non-dimensional axial location of groove	$\Delta SM$	stall margin improvement
CFD	computational fluid dynamics	$\Delta \eta_{peak}$	variation in peak efficiency
CT	casing treatment	$\eta$	adiabatic efficiency
$c_x$	axial tip chord		
d	depth of groove		
LE	leading edge of blade		
$\dot{m}$	mass flow rate		
PR	total pressure ratio		
SM	stall margin		
TE	trailing edge of blade		
w	non-dimensional width of groove		
x	axial location		
$y^+$	non-dimensional wall distance		
		<b>Subscripts</b>	
		ave	average
		GW	Grooved Wall
		max	maximum
		min	minimum
		peak	peak adiabatic efficiency point
		stall	near-stall point
		SW	smooth wall

## 1. INTRODUCTION

In a gas turbine engine, the stable operation of the compressor has vital effect on the stable operating range of the whole engine. Casing treatment (CT) is a well-known passive control method that could be implied to improve the stable operating range of the

axial-flow compressors and fans.

Various configurations such as porous casing, axial slot and circumferential groove have been studied by experimental and numerical methods since early 1960. Moore *et al.* (1971) examined some casing treatment configurations and found that the circumferential groove could improve the stall

margin and the peak efficiency of an axial-flow compressor rotor. Greitzer *et al.* (1979) supposed the hypothesis that the casing treatment is effective only in a situation in which a wall stall exists. Crook *et al.* (1993) numerically explored the effect of the grooved casing in suppressing the stall and identified two principal effects: suction of the high blockage fluid at the rear of the passage and energizing of the tip leakage flow. Some researchers (Puterbaugh *et al.* 1997; Furukawa *et al.* 1998) indicated that the tip leakage flow and its interaction with passage shock wave, has an important role in the transonic compressor aerodynamics. Furakawa *et al.* (2000) showed that the tip leakage vortex breakdown could be one the sources of unsteadiness in the compressor. Wilke and Kau (2002) through a numerical study showed that the tip leakage vortex breakdown lead the compressor to stall and the casing treatments has ability to delay the vortex breakdown and move the surge line to the lower mass flows. Ito *et al.* (2008) concluded from numerical simulations that circumferentially contouring endwall above the blade leading edge had the significant stall margin improvement by weakening the rotating instability vortex. Vo *et al.* (2008) based on unsteady simulation proposed that the leading edge spillage and the trailing edge back flow are two conditions necessary for triggering the spike type stall, both of which are linked to the tip leakage vortex. Chen *et al.* (2008) showed that the spike instabilities occur when the trajectory of the tip clearance flow becomes perpendicular to the axial direction. Legras *et al.* (2010) studied on the effect of circumferential grooves on the tip leakage flow and its resulting vortical flow structures. They observed that the grooves could change the trajectory of tip leakage vortex and in addition generate a set of secondary tip leakage vortices. Shabbir and Adamczyk (2005) analyzed the balance of the axial momentum near a grooved casing to explain the effective mechanism of circumferential groove. They found that the radial transport of the axial momentum imparted by the groove could reduce the growth rate of blockage and accordingly increase the stall margin. Chen *et al.* (2014) verified the ability of unmatched grid approaches in simulation of the casing treatment and showed that circumferential grooves could reduce the backward axial momentum flux in the gap flow and accordingly extend the stall margin of the compressor. Legras *et al.* (2012) presented a generalized method of Shabbir's approach to reveal the flow mechanisms induced by any CT geometry. Their results indicate that the axisymmetric CT is characterized by its bleeding effect and the slot-type CT is characterized by both a bleeding effect at the rear-part and the blowing effect at the front-part of the compressor. Kroeckel *et al.* (2011) carried out an experimental investigation on the application of a multistage CT in a 2.5 stage axial compressor and confirmed that multistage CT is able to push the surge line towards higher pressure ratios and lower mass flow rates significantly with negligible decline in the peak efficiency. Ramzi and AbdErrahmane (2013) simulated a slotted cascade and showed its ability to reduce the secondary flow structures and eliminate the boundary layer separation at midspan and the corner stall. Taghavi and Eslami (2013) used

the large eddy simulation and showed that the casing treatment reduces the amplitude of the unsteadiness of the tip leakage flow and gets its frequency closer to the blade passing frequency that lead to reduction of blockage and losses as a result. Kim *et al.* (2012, 2013) conducted a multi-objective optimization based on the steady flow analysis to reach the best configuration of the five circumferential grooves. Also they studied the effect of number and shape of circumferential groove in other papers. Sakuma *et al.* (2014) numerically studied the effect of varying the axial location and the depth of a single circumferential groove on the stability improvement of NASA Rotor 37. They explained higher potential of deeper grooves in the stability enhancement, and the best position for the groove to be located was pointed out to exist near the blade leading edge.

This paper aims to understand the effect of a single shallow circumferential groove CT on the stability enhancement and the flow structure in the tip region of a well-known axial transonic compressor, NASA Rotor 37. The depth of groove was chosen a value smaller than the selected value by some researchers (Kim *et al.* 2013, Sakuma *et al.* 2014 and etc.). A parametric study was conducted on the width and the axial location of the groove. Steady state simulations of the compressor with various grooves were done and the results were compared with the simulation of compressor without groove. To evaluate the effect of the groove on the near-tip flow structure, smooth wall condition and some cases with maximum stall margin improvement were discussed by details.

## 2. TRANSONIC COMPRESSOR ROTOR

As previously mentioned, NASA Rotor 37, has been used in the present study. The rotor was designed and tested by NASA Lewis Research Center in the late 1970's. The specification of the rotor has been summarized in the Table 1 (Dunham 1998). At the design point, the total pressure ratio is 2.106 and the mass flow is 20.19 kg/s. The choking mass flow is 20.93 kg/s, and the near-stall point is 0.925 of the choked flow. At the design speed of 17,188.7 rpm, the inlet relative Mach number at the hub and the tip is 1.13 and 1.48 respectively. The measured tip clearance is 0.356 mm at the design speed. The overall performance and radial distributions of total pressure and total temperature were obtained at station 1 and station 4 (Fig. 1) and were used for the validation of numerical simulation.

**Table 1 Design specifications of NASA Rotor 37**

Blade Number	36
Blade profile	Multiple Circular Arc
Blade tip radius (mm)	252
Blade tip speed (m/s)	454
Hub-tip ratio	0.7
Aspect ratio	1.19
Solidity at tip	1.288

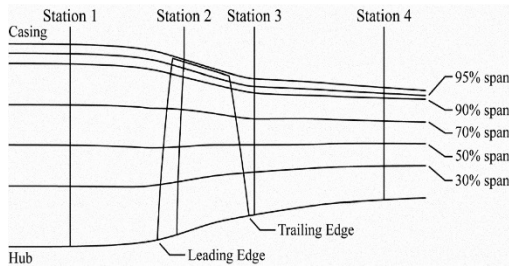


**Fig. 1. NASA rotor 37 measurement locations in experiment.**

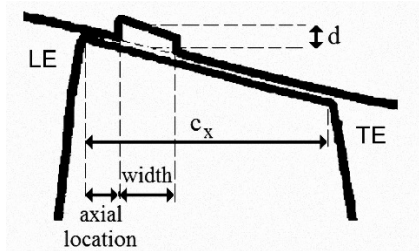


**Fig. 2. Schematic of the circumferential groove.**

**Table 2 Groove geometry data.**

w	A	Number of locations
5	0, 10, 20, 30, 40, 50, 60, 70, 80, 90	10
10	0, 10, 20, 30, 40, 50, 60, 70, 80, 90	10
20	0, 10, 20, 30, 40, 50, 60, 70, 80	9
40	0, 10, 20, 30, 40, 50, 60	7
60	0, 10, 20, 30, 40	5
80	0, 10, 20	3
100	0	1

### 3. GEOMETRY OF CIRCUMFERENTIAL GROOVES

In the present research, a parametric study was conducted on the width and the axial location of a single circumferential groove. Some researchers studied the effect of circumferential grooves with depth of 12 times the rotor tip clearance on the performance of rotor 37 (Kim *et al.* 2012, 2013; Huang *et al.* 2008). Since deeper groove needs thicker casing that could impose additional weight on the engine and this is not suitable in aviation applications, therefore in this study the groove was considered to be shallow and the depth was fixed to 3 times the rotor tip clearance. The schematic of the groove has been shown in Fig. 2. It has been considered that the groove must be located on the top of the blade between the leading edge and the trailing edge. Also the upper limit of axial location of the groove depends on the width of the groove. The axial location and the width of the groove were normalized by the tip axial chord of the rotor. The value of non-dimensional axial location and non-dimensional width of the groove have been presented in Table 2. According to the Table 2, forty five various configurations were created. Each configuration was

distinguished by the combination of two numbers, which specified as “a” and “w”. For example, a groove with a=30 and w=5 was named “Config-a30-w5”.

## 4. NUMERICAL ANALYSIS METHOD

### 4.1 Numerical Scheme

Steady Reynolds-averaged Navier-Stokes (RANS) equations were solved using a commercial three-dimensional solver package. The two-equation  $k-\omega$  shear stress transport (SST) turbulence model was utilized to produce accurate results for the flow near the wall. This model combines the  $k-\omega$  model near the wall and the  $k-\epsilon$  model away from the wall. In combination with the SST model, an automatic wall treatment was used which gradually switches from a classical low-Reynolds formulation on fine grids to a logarithmic-wall function on coarse grids (Menter *et al.* 2003; Menter 2009). This automatic switch of the wall function reduces the stringent grid resolution required for standard low-Reynolds turbulence models. Solid boundaries representing the moving and the stationary walls were considered to be smooth and adiabatic. The periodic boundary condition was used to simulate only single blade domain. The general grid interface (GGI) method was applied for unmatched interface between the passage domain and the circumferential groove. At the inlet boundary, the total pressure, the total temperature, and the flow angle were imposed. The mass flow rate of compressor was calculated explicitly by setting the hub static pressure at outlet and using radial equilibrium to compute spanwise distribution of the static pressure.

To calculate near-choke condition, a relatively low value for the exit static pressure was selected. Other points of the characteristic map obtained through increase in the outlet static pressure. The stalling point of the compressor was found by examining the iteration history of the computations. The lowest possible mass flow rate condition that was found to converge to a stable solution was determined to be the near-stall point. After the near-stall point, a continual drop in the mass flow rate and the total pressure ratio occurs with increasing iteration count that is known as numerical stall (Ito *et al.* 2008). To predict the near-stall point accurately, the increment of the outlet static pressure near the stall was selected 150 Pascal. The near-stall point and numerical stall point of smooth wall condition obtained through imposing the outlet static pressure on 122.45 and 122.6 kPa respectively. This technique of finding the stalling mass flow rate using RANS solutions has been used by many researchers (such as Ito *et al.* 2008; Kim *et al.* 2013; Sakuma *et al.* 2014). However, the limitation of this method was noted that the stall is not properly modeled using RANS solutions because of its inherently unsteady phenomenon.

### 4.2 Computational Grid

In order to study the effect of grid size on the simulation, three structured mesh were created in the rotor passage domain with the O-grid topology near

the blade surface and the H/J/C/L topology in the other regions. As shown in Fig. 3, the values of the total pressure ratio, the adiabatic efficiency of the compressor and normalized mass flow rate of near-stall point have only slight changes with the variation of grid size from 471154 to 934448 nodes. Thus, the grid of 471154 nodes was selected to do this study. The computational domain of the compressor passage has 99 axial, 59 tangential and 79 radial points. The tip clearance has 15 nodes in radial direction to simulate the tip leakage flow. The minimum wall distance was set to  $4 \times 10^{-6}$  (m) which gave  $y^+ < 5$  at solid walls. The value of  $y^+$  on the 4 critical surfaces was summarized in the Table 3 for the three different grid sizes.

**Table 3  $y^+$  value on surfaces**

Surface name		258284 nodes	471154 nodes	934448 nodes
Suction side	$y_{min}^+$	0.3	0.09	0.02
	$y_{max}^+$	9.52	4	1.66
	$y_{ave}^+$	5.18	1.9	0.94
Pressure side	$y_{min}^+$	0.27	0.16	0.03
	$y_{max}^+$	12.7	4.6	1.93
	$y_{ave}^+$	6.43	2	1.05
hub	$y_{min}^+$	0.2	0.09	0.03
	$y_{max}^+$	9.35	4.8	1.68
	$y_{ave}^+$	5.14	1.98	0.97
shroud	$y_{min}^+$	1.08	0.4	0.24
	$y_{max}^+$	8.51	4.2	1.9
	$y_{ave}^+$	4.05	1.95	1.64

Also a structured mesh with about 120000 nodes was created in the groove domain with 61 tangential, 21 radial and average 93 axial points. The whole computational grid has been shown in Fig. 4.

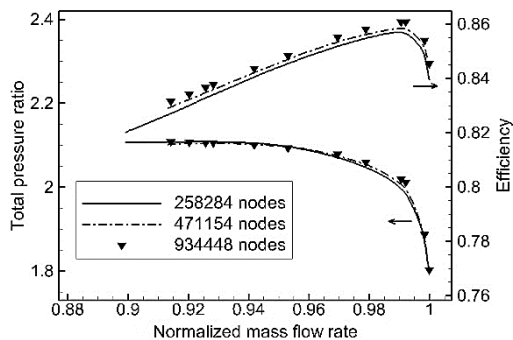


**Fig. 3. Effect of grid size on characteristic maps of compressor.**

### 4.3 Validation

In order to verify numerical simulations, the results of the simulation of smooth wall condition were validated against the experimental data of NASA rotor 37 (Dunham 1998). Numerical spanwise distribution of the total pressure ratio and the total

temperature ratio at station 4 (Fig. 1) were compared with the experimental one (Fig. 5) at near peak efficiency condition (98% of choke mass flow rate). It can be seen that there is a good agreement between the numerical and the experimental data. Since the cavity between the rotating rotor hub and the fixed hub was not simulated, the total pressure ratio and the total temperature ratio near the hub are greater than experimental values. Similar results have been reported by others (Dunham 1998).

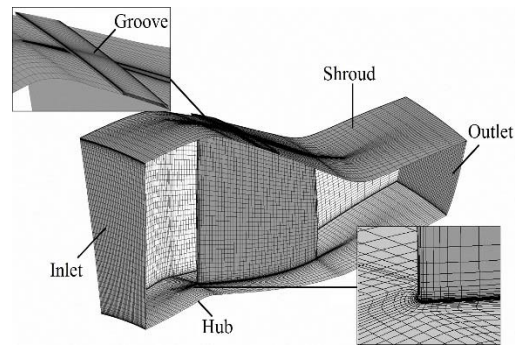


**Fig. 4. Computational grid.**

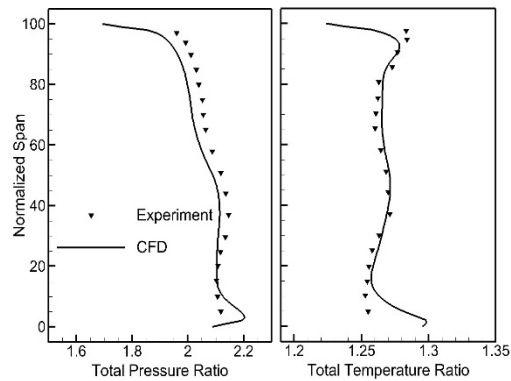


**Fig. 5. Spanwise distribution of total pressure ratio and total temperature ratio.**

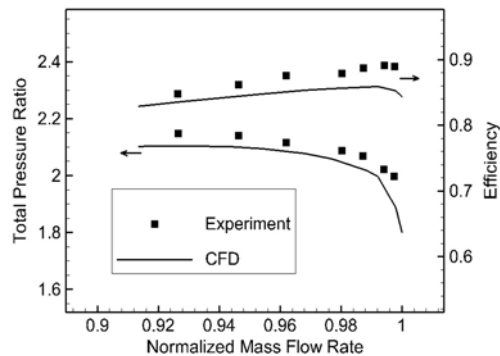


**Fig. 6. Characteristic map of rotor.**

Also the characteristic maps of the rotor at design speed have been presented in Fig. 6. It shows uniform underestimations of the total pressure ratio and the adiabatic efficiency through the entire range of normalized mass flow rate ( $\dot{m} / \dot{m}_{choke}$ ) by a good agreement with the experimental data.

The predicted near-stall point determined by simulation is 0.913 of the choked flow which is 0.012 smaller than the measured value but on the whole, the numerical method could predict the flow with sufficient reliability.

## 5. RESULTS AND DISCUSSION

### 5.1 Effect of Groove on Stall Margin and Peak Efficiency

The stall margin of an axial-flow compressor is defined as follow (Kim *et al.* 2013):

$$SM = \left( \frac{\dot{m}_{peak}}{\dot{m}_{stall}} \times \frac{PR_{stall}}{PR_{peak}} - 1 \right) \times 100 \% \quad (1)$$

According to the Eq. 1, the stall margin of the compressor with smooth wall condition was calculated 13.51%. To demonstrate the effects of the groove on the stall margin and the peak efficiency, their variation were evaluated as below:

$$\Delta SM = SM_{GW} - SM_{SW} \quad (2)$$

$$\Delta \eta_{peak} = \eta_{peak_{GW}} - \eta_{peak_{SW}} \quad (3)$$

Figure 7 shows the effect of the groove on the stall margin improvement for various configurations. As shown in Fig. 7, for all values of the groove width, stall margin decreased when the groove was located exactly on the top of the blade leading edge ( $a=0\%$ ). Narrow grooves ( $w=5\%$ ,  $10\%$ ) had maximum stall margin improvement when were placed next to the blade leading edge ( $a=10\%$ ). At this condition, the leading edge of the groove is located before the position of the interaction between the shock wave and the tip leakage vortex. As described on the next sub-section, these grooves could reduce the size of blockage produced by the vortex breakdown.

Also according to the simulation results in the near-stall point, the shock wave interacts with the blade suction side boundary layer and leads it to separate at about 30% of the axial chord. This position seems to be important in Fig. 7. The grooves with  $w=20\%$ , could increase the stall margin at all locations except the leading edge and reached into maximum when  $a=30\%$ . Also mid-width grooves ( $w=40\%$ ,  $60\%$ ) over the aft-part of the blade ( $a < 30\%$ ), had negative effect on the stability but by shifting the groove toward the mid-part of blade ( $a \geq 30\%$ ), good stability enhanced so that the maximum stall margin obtained by Config-a40w40. This type of behavior refers to the effect of the groove on the blade suction side separation described on the next sub-section.

Figure 8 shows the effect of the groove on the peak efficiency of the compressor for various configurations. It is seen that narrow grooves had slight effect on the peak efficiency. However the peak efficiency decreased according to the increase of the groove width. Any groove located on the top of the blade leading edge ( $a=0\%$ ), reduced the peak efficiency of compressor.

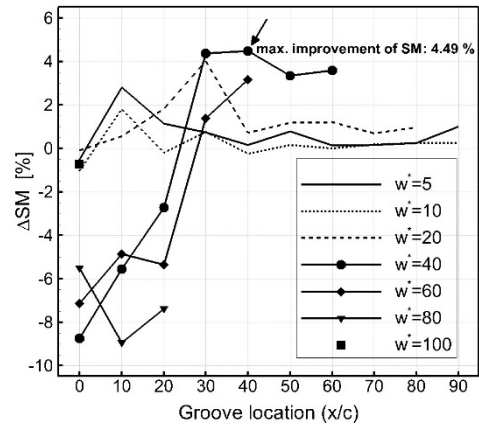


Fig. 7. Effect of groove on stall margin.

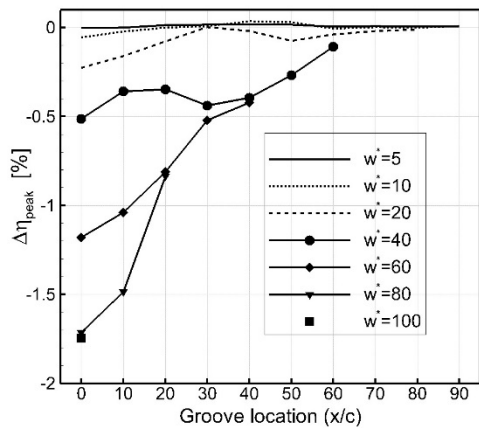
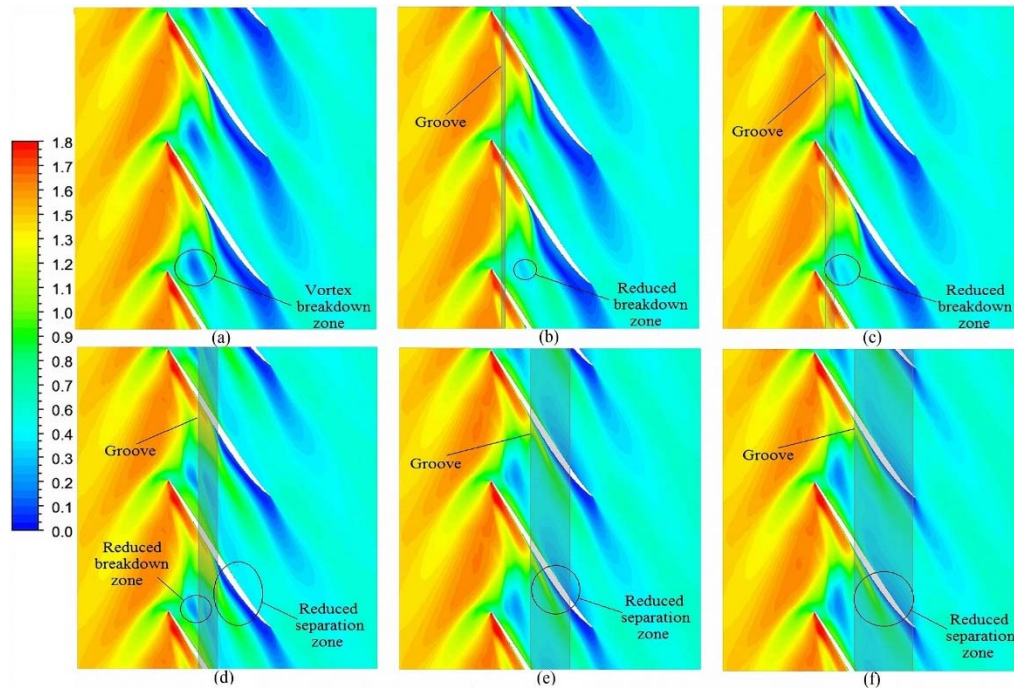


Fig. 8. Effect of the groove on the peak efficiency.

### 5.2 Effect of the Groove on the Flow Field

In this part of the paper, the effect of the groove on the flow field of compressor has been described for some configurations to demonstrate how a CT could improve the compressor stability. For any individual groove width, only one groove was selected on the basis of maximum stall margin improvement. Therefore according to Fig.7, five configurations were selected as follows: Config-a10w5, Config-a10w10, Config-a30w20, Config-a40w40 and Config-a40w60. The comparisons between the grooved wall and the smooth wall condition were done at the near-stall point of the smooth wall condition (mass flow rate of 19.15 kg/s).

Figure 9 shows the relative Mach contours at the 98% span. In a transonic compressor, when the mass flow rate reduces, the intensity of the interaction between the shock wave and the tip leakage vortex increases, so the vortex core expands through passing the shock wave and generates a vortex breakdown zone. This blockage region leads the compressor toward the stall as reported by other researchers (Wilke and Kau 2004; Sakuma *et al.* 2014). It has been shown in Fig.9 that narrow grooves have the ability to reduce the size of vortex breakdown zone. Also Fig. 9 shows that medium-width grooves have another mechanism to delay the stall. These grooves have ability to weaken the



**Fig. 9. Relative Mach contours at 98% span at near-stall point of the smooth wall; (a) smooth wall, (b) Config-a10w5, (c) Config-a10w10, (d) Config-a30w20, (e) Config-a40w40, (f) Config-a40w60.**

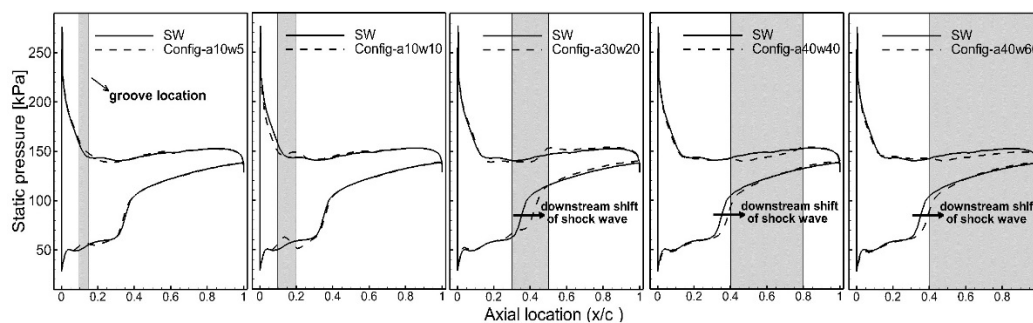


**Fig. 10. Static pressure distributions on the blade at 98% span at near-stall point of the smooth wall.**

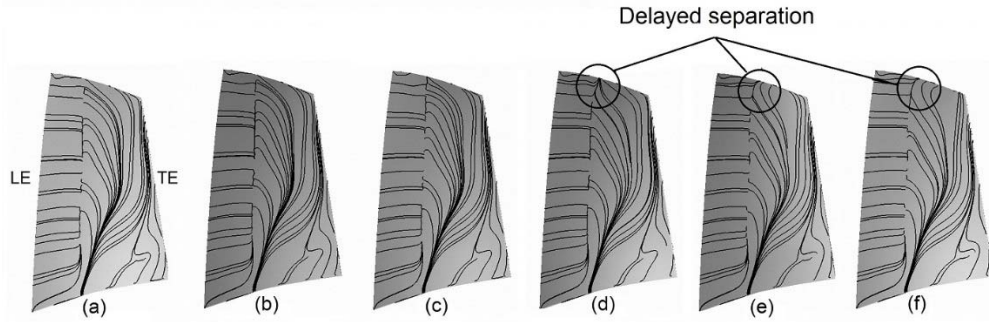
interaction between the shock wave and the boundary layer and so reduce the size of separation zone on the suction side of the blade. However it seems that, not only vortex breakdown but also blade suction side separation at the tip region has important effect on the stall of the compressor.

Figure 10 compares the static pressure distributions on the blade pressure and suction sides at 98% span for the smooth wall and some grooved wall configurations. The gray zones in the figure show the location of the groove. All grooves have reduced the blade loading at its own location, in the other hand, the static pressure difference between the pressure side and the suction side of the blade has decreased locally at the groove location. This local reduction of the blade loading could affect the tip leakage flow. At the suction side of the blade, the static pressure has been increased suddenly by shock wave. Also Fig. 10 shows that some grooves have shifted the shock wave toward downstream. As the shock wave

moves downstream, the interaction between the shock wave and the blade boundary layer takes place later and accordingly a delayed separation on the blade suction side occurs. Therefore the size of the blockage near the blade trailing edge reduces. The delayed separation near the blade tip has been shown by black circles in Fig. 11.

### 5.3 Effect of the Groove on the Compressor Characteristic Map

Figure 12 shows the effect of some selected grooves on the characteristic map of the compressor. The important result of this figure is that wider grooves reduce the total pressure ratio and the adiabatic efficiency of compressor through the whole speed-line and narrow grooves don't have sensible effect on it regardless of their positive effect on the stall mass flow rate. All of these selected grooves have negligible effect on the choke flow rate but could move the stall point to the lower mass flow rates relative to the smooth wall condition.



**Fig. 11.** Streamlines on blade suction surface at near-stall point of the smooth wall condition; (a) smooth wall, (b) Config-a10w5, (c) Config-a10w10, (d) Config-a30w20, (e) Config-a40w40, (f) Config-a40w60.

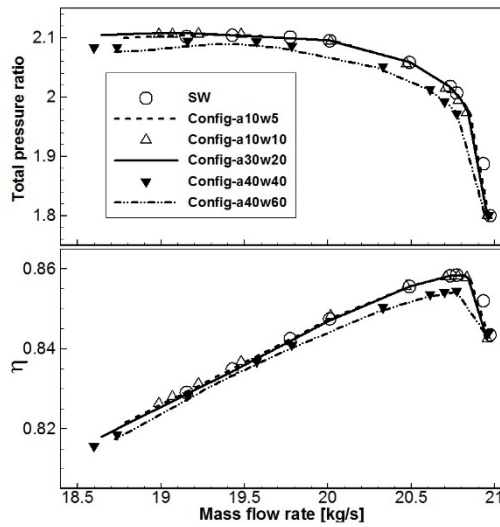


**Fig. 12.** Characteristic map of compressor.

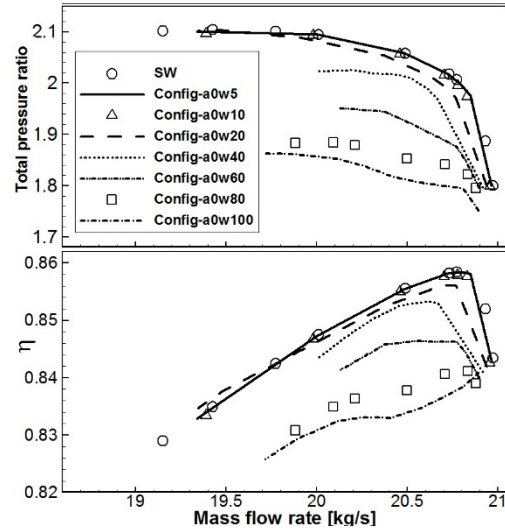


**Fig. 13.** Characteristic map of compressor for grooves that were located at  $a=0\%$ .

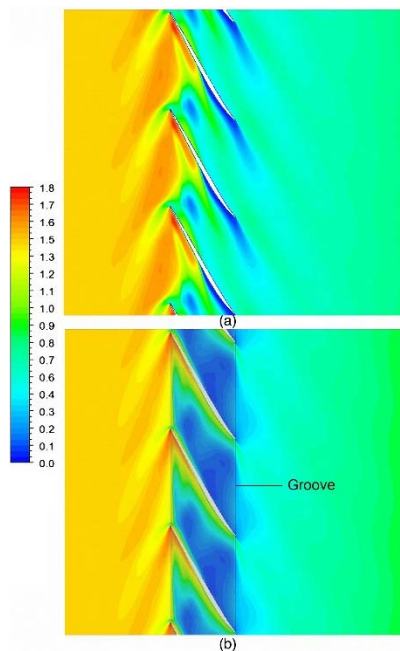


**Fig. 14.** Relative Mach contours at 98% span at near-stall point of Config-a0w100; (a) smooth wall, (b) Config-a0w100.

#### 5.4 Negative Effect of Some Grooves

As it was mentioned before, the stall margin and the peak efficiency of the compressor reduced when a groove was located exactly at the axial location of the blade leading edge ( $a=0\%$ ). Fig. 13 shows the characteristic map of the compressor for this type of grooves. Figure 13 shows the slight changes of the choke mass flow rate utilizing these grooves. Also according to Fig. 13, the groove which whose width is equal or smaller than 20% of the tip axial chord, only reduces the stall margin and its effect on the total pressure ratio and the efficiency is small. But the groove which whose width is greater than 20%, not only reduces the stall margin, but also reduces the total pressure ratio and the efficiency of the compressor significantly so that the maximum decline occurs using Config-a0w100. Effect of this configuration on the compressor behavior is similar to the effect of increased tip gap size on the behavior of Rotor 37 that was investigated by Beheshti *et al.* (2004). They demonstrated that large tip gap has detrimental effects on the pressure rise, stability, and efficiency of the compressor.

Figure 14 shows relative Mach contours at span 98% at the near-stall point of Config-a0w100 (19.7 kg/s).

It reveals that a large blockage region has happened near the tip region. This blockage is created by increased tip leakage flow and has some effects on the flow such as: suppress the energy transport from the blade to the fluid, increase the inlet flow angle and increase the loss of the secondary flows. Also the blockage leads the compressor to go ahead the stall at higher mass flow rate.

## 6. CONCLUSION

Steady RANS simulations were conducted to study the effect of single shallow circumferential casing treatment on the flow field and the stability of NASA Rotor 37. The conclusions are summarized below:

1. Any groove, whose leading edge had the same axial location of the blade leading edge, causes negative effects on the compressor characteristics, for instance, the peak efficiency and the stall margin.
2. Some narrow grooves had slight effect on the peak efficiency of the compressor especially when located on the top of the blade mid-part. As the width of the groove was increased, the peak efficiency of compressor decreased, that is, the wider the groove, the lower the efficiency and the total pressure ratio occurs in the whole speed line.
3. It was found that not only the vortex breakdown but also the blade suction side separation at the tip region has important effect on the compressor stall.
4. It was observed that when the narrow groove was located before the interaction position between the shock wave and the tip leakage vortex, the size of blockage produced by vortex breakdown decreased and accordingly the stall occurred at the lower mass flow rate.
5. Also it was noted that when medium-width grooves were located above the interaction position between the shock wave and the blade boundary layer, the size of blockage produced by the separation on the blade suction side decreased and accordingly the stall occurred at the lower mass flow rate.
6. Finally, single shallow circumferential groove displayed the desirable capacity to improve the stability of the compressor. It should be pointed out that, to a large extent, the width determines where the groove should be located.

## ACKNOWLEDGEMENTS

The authors would like to thank Jin-Hyuk Kim for helping on some aspects of simulations.

## REFERENCES

Beheshti, B. H., J. A. Teixeira, P. C. Ivey, K. Ghorbanian and B. Farhanieh (2004). Parametric study of tip clearance-casing treatment on performance and stability of a

transonic axial compressor. *Journal of Turbomachinery* 126(4), 527-535.

- Chen, H., X. Huang, K. Shi, S. Fu, M. Ross, M. A. Bennington and *et al.* (2014). A computational fluid dynamics study of circumferential groove casing treatment in a transonic axial compressor. *Journal of Turbomachinery* 136(3).
- Chen, J. P., M. D. Hathaway and G. P. Herrick (2008). Prestall behavior of a transonic axial compressor stage via time-accurate numerical simulation. *Journal of Turbomachinery* 130(4).
- Crook, A. J., E. M. Greitzer, C. S. Tan and J. J. Adamczyk (1993). Numerical simulation of compressor endwall and casing treatment flow phenomena. *Journal of Turbomachinery* 115, 501-512
- Dunham, J. (1998). *CFD validation for propulsion system components* (1a validation CFD des organes des propulseurs). *DTIC Document*.
- Furukawa, M. *et al.* (2000). Unsteady flow behavior due to breakdown of tip leakage vortex in an axial compressor rotor at near-stall condition. *ASME turbo expo: Power for land, sea, and air, American Society of Mechanical Engineers*.
- Furukawa, M., M. Inoue, K. Saiki and K. Yamada (1998). The role of tip leakage vortex breakdown in compressor rotor aerodynamics, *ASME 1998 Int. Gas Turbine Aeroengine Congr. Exhib, American Society of Mechanical Engineers*.
- Greitzer, E. M., J. P. Nikkanen, D. El Haddad, R. S. Mazzawy and H. D. Joslyn (1979). A fundamental criterion for the application of rotor casing treatment. *J. Fluids Eng.* 101, 237-243.
- H. D. Vo, C. S. Tan, E. M. Greitzer (2008). Criteria for spike initiated rotating stall, *Journal of turbomachinery*, 130, 11023.
- Huang, X., H. Chen and S. Fu (2008). *CFD investigation on the circumferential grooves casing treatment of transonic compressor. ASME turbo expo 2000: Power for land, sea, and air, American Society of Mechanical Engineers*.
- Wilke I., H. P. Kau (2004). A Numerical Investigation of the Flow Mechanisms in a High Pressure Compressor Front Stage with Axial Slots, *Journal of turbomachinery*, 126, 339.
- Ito, Y., T. Watanabe, and T. Himeno (2008). Numerical investigation of contoured endwall effects in a transonic. *International Journal of Gas Turbine, Propulsion and Power Systems* 2(1), 24-29.
- Kim, J. H., K. J. Choi and K. Y. Kim (2012). Performance evaluation of a transonic axial compressor with circumferential casing grooves. In *Proceedings of the Institution of Mechanical Engineers, Part A: Journal of Power and Energy* 226(2), 218-230.

- Kim, J. H., K. J. Choi and K. Y. Kim (2013). Aerodynamic analysis and optimization of a transonic axial compressor with casing grooves to improve operating stability. *Aerospace Science and Technology* 29(1), 81-91.
- Kim, J. H., K. Y. Kim and K. Cha (2013). Effects of number of circumferential casing grooves on stall flow characteristics of a transonic axial compressor. *Applied Mechanics and Materials* 284.
- Kroeckel, T. S. J. Hiller and P. Jeschke (2011). *Application of a Multistage Casing Treatment in a High Speed Axial Compressor Test Rig*, ASME Turbo Expo: Turbine Technical Conference and Exposition, American Society of Mechanical Engineers.
- Legras, G., I. Trébinjac, N. Gourdain, X. Ottavy and L. Castillon (2012). A novel approach to evaluate the benefits of casing treatment in axial compressors. *International Journal of Rotating Machinery*.
- Legras, G., N. Gourdain and I. Trebinjac (2010). Numerical analysis of the tip leakage flow field in a transonic axial compressor with circumferential casing treatment. *Journal of Thermal Science* 19(3), 198-205.
- Menter, F. R. (2009). Review of the shear-stress transport turbulence model experience from an industrial perspective. *International Journal of Computational Fluid Dynamics* 23(4), 305-316
- Menter, F., J. C. Ferreira, T. Esch and B. Konno (2003). The SST turbulence model with improved wall treatment for heat transfer Predictions in Gas Turbines. In *Proceedings of the International Gas Turbine Congress, Tokyo*.
- Moore, R. D., G. Kovich and R. J. Blade (1971). Effect of casing treatment on overall and blade-element performance of a compressor rotor. *National Aeronautics and Space Administration*.
- Puterbaugh, S. L. and M. Brendel (1997). Tip clearance flow-shock interaction in a transonic compressor rotor. *Journal of Propulsion and Power* 13, 24–30.
- Ramzi, M. and G. AbdErrahmane (2013). Passive control via slotted blading in a compressor cascade at stall condition. *Journal of Applied Fluid Mechanics* 6(4), 571-580.
- Sakuma, Y., T. Watanabe, T. Himeno, D. Kato, T. Murooka and Y. Shuto (2014). Numerical analysis of flow in a transonic compressor with a single circumferential casing groove-influence of groove location and depth on Flow instability. *Journal of Turbomachinery* 136.
- Shabbir, A. and J. J. Adamczyk (2005). Flow mechanism for stall margin improvement due to circumferential casing grooves on axial compressors. *Journal of Turbomachinery* 127(4), 708-717.
- Taghavi-Zenouz, R. and S. Eslami (2013). Effects of casing treatment on behavior of tip leakage flow in an isolated axial compressor rotor blade row. *Journal of the Chinese Institute of Engineers* 36(7), 819-830.
- Wilke, I. and H. P. Kau (2002). A numerical investigation of the influence of casing treatments on the tip leakage flow in a HPC front stage. *ASME Turbo Expo Power Land, Sea, Air*. 1–11.